Inorg. Chem. **2007**, *46*, 6319–6328

Chemical Bonding in $TiSb_2$ and VSb_2: A Quantum Chemical *and* Experimental Study

Marc ArmbrUster,* Walter Schnelle, Ulrich Schwarz, and Yuri Grin

Max-Planck-Institut für Chemische Physik fester Stoffe, Nöthnitzer Str. 40, 01187 Dresden, Germany

Received February 12, 2007

The chemical bonding in the isostructural intermetallic compounds $TiSb_2$ and VSb_2, crystallizing in the $CuAl_2$ type, was investigated by means of quantum chemical calculations, particularly the electron localization function (ELF), as well as by Raman spectroscopy, Hall effect and conductivity measurements on oriented single crystals, and high-pressure X-ray powder diffraction. The homogeneity ranges of the compounds were determined by powder X-ray diffraction, WDXS, and DSC measurements. $TiSb_2$ exhibits no significant homogeneity range, while VSb_2 shows a small homogeneity range of approximately 0.3 at. %. According to the ELF calculations, the Sb atoms form dumbbells via a two-center two-electron bond, while the T atoms (T = Ti, V) build up chains along the crystallographic *c*-axis. Both building units are connected by covalent T–Sb–T three-center bonds, thus forming a three-dimensional network. The strength of the bonds involving Sb was determined by fitting a force constant model to the vibrational mode frequencies observed by polarized Raman measurements on oriented single crystals. The resulting bond order of the Sb_2 dumbbells is 1, while the strength of the three-center bonds resembles a bond order of 1.5. The weak pressure dependence of the *c*/*a* ratio confirms the slightly different bonding picture in $TiSb_2$ compared to that in $CuAl_2$. Electrical transport measurements show the presence of free charge carriers, as well as a metal-like temperature dependence of the electrical resistivity.

Introduction

The two antimonides $TiSb_2$ and VSb_2 were synthesized for the first time in 1951 by Nowotny, Pesl, and Funk.[1,2] The crystal structures were reinvestigated recently, revealing a vanadium-deficient site in VSb_2.[3] Both compounds crystallize in the tetragonal crystal structure of the $CuAl_2$ type, comprising transition metal atoms coordinated by eight main group atoms forming a square antiprism. The antiprisms are forming columns along [001] by sharing quadratic faces. In addition, they share edges which results in a linkage of neighboring columns in the (001) plane (Figure 1).

Several authors discussed the chemical bonding of VSb_2 and $TiSb_2$.[1,2,4,5,6] In the early publications, these discussions were solely based on geometrical considerations, that is, the distances between the atoms. The short Sb−Sb distance *d*1 implies the formation of Sb_2 dumbbells. The Mössbauer measurements showed significant T−Sb (T = Ti, V)

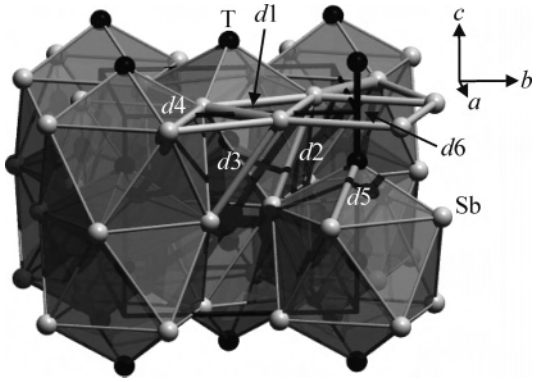

Figure 1. Crystal structure of $TiSb_2$ and VSb_2 showing edge-sharing columns of base-stapled quadratic $TSb_{8/4}$ antiprisms (T = Ti, V). The shortest Sb−Sb (*d*1−*d*4), T−Sb (*d*5), and T−T (*d*6) distances are shown.

* To whom correspondence should be addressed. Phone: +44(0)1223/33 65 33. Fax: +44(0)1223/33 63 62. E-mail: research@armbruester.net. Current address: University of Cambridge, Chemistry Department, Lensfield Road, Cambridge CB2 1EW, U.K.

(1) Nowotny, H.; Funk, R.; Pesl, J. *Monatsh. Chem.* **1951**, *82*, 513−525.
(2) Nowotny, H.; Pesl, J. *Monatsh. Chem.* **1951**, *82*, 336−343.
(3) Armbrüster, M.; Cardoso Gil, R.; Burkhardt, U.; Grin, Yu. *Z. Kristallogr.—New. Cryst. Struct.* **2004**, *219*, 209−210.
(4) Dashjav, E.; Kleinke, H. *J. Solid State Chem.* **2003**, *176*, 329−337.
(5) Donaldson, J. D.; Kjekshus, A.; Nicholson, D. G.; Rakke, T. *J. Less-Common Met.* **1975**, *41*, 255−263.
(6) Havinga, E. E.; Damsma, H.; Hokkeling, P. *J. Less-Common Met.* **1972**, *27*, 169−186.

10.1021/ic070284p CCC: $37.00
Published on Web 07/11/2007

bonding, in addition to the Sb−Sb interactions.[5] This picture of the chemical bonding is supported by COHP calculations of Dashjav and Kleinke[4] which showed that the compounds exhibit homoatomic, as well as heteroatomic, bonding interactions. The chemical bonding in the prototype compound $CuAl_2$ was analyzed recently by several techniques.[7,8] These investigations lead to the description of $CuAl_2$ as interpenetrating graphite-like nets of covalently bonded aluminum atoms (two-center (2c) bonds) with embedded Cu atoms connected to the aluminum nets via three-center Cu−Al−Cu bonds. The main aim of the present work is to find out how far this bonding pattern can be transferred from $CuAl_2$ to the isostructural antimonides of titanium and vanadium.

Since no reliable information about the stability ranges of the compounds is available, we started our investigations by studying their homogeneity ranges. The combination of quantum chemical calculations, especially the electron localization function (ELF) and physical property measurements, like polarized Raman spectroscopy on single crystals, was employed to gain a physically meaningful description of the chemical bonding with respect to its kind and strength.

Experimental Section

Preparation. Single-phase powder samples of the compounds, as well as two-phase samples, were prepared by mixing and pressing pellets of appropriate amounts of fine powders of the elements (Ti, AlfaAesar 99+%; V, ChemPur 99.5%; Sb, ABCR 99.999%) in a glovebox. Since the vanadium was not delivered under an inert atmosphere, it was cleaned with aqueous 10% HCl solution prior to the experiments.[9] After the pellets were enclosed in evacuated quartz glass ampules, they were subjected to a heat treatment at 640 °C for 10−30 days, in the case of the pure compounds, and 700 °C for several weeks, in the case of the two-phase samples. Subsequently, the ampules were quenched in water to room temperature.

Large single crystals (up to several mm) could be obtained by melting the compounds with excess antimony (ratio T/Sb = 1:10) at 1000 °C and homogenizing the melt for 6 h. After the melt was cooled in 240 h to 620 °C, the oven was switched off to allow the samples to cool down slowly to ambient temperature. Afterwards, the excess antimony was sublimed within 24 h to the top of the ampules, leaving behind well-shaped prismatic crystals of the diantimonides with a dark metallic luster and prismatic morphology.

X-ray Diffraction. X-ray powder diffraction experiments were conducted on a Huber image plate camera G670 with Cu $K\alpha_1$ radiation (Guinier geometry, SiO_2 monochromator, $\lambda_{Cu} = 1.540562$ Å) and Ge as internal standard ($a = 5.65752$ Å). The samples were finely ground and spread on a 6 μm thick Mylar foil (Chemplex) coated with Vaseline. Lattice parameters were refined on definite sets of 28 and 30 reflections for $TiSb_2$ and VSb_2, respectively, with the program WinCSD.[10]

Single-crystal structure determination for both compounds was performed on an R-AXIS RAPID diffractometer (Rigaku/MSC) in Weissenberg geometry. The diffractometer was equipped with a graphite monochromator and a Mo X-ray tube ($\lambda_{Mo} = 0.71073$ Å, 50 kV, 40 mA). The measurement was followed by a numerical absorption correction. The crystal structure was solved and refined against F^2 by using the SHELX-97[11,12] software as implemented in the WinGX[13] program package.

High-pressure diffraction experiments were performed at beamline ID09 at the ESRF, Grenoble. A fine powder, prepared by grinding single crystals of $TiSb_2$, was placed in a tungsten gasket together with paraffin as pressure-transfer medium. High pressures were generated by diamond anvil cells (Diacell Products) equipped with beryllium backing plates. Pressure calibration was performed by means of the ruby luminescence method.[14] Diffraction patterns were recorded up to 30° in 2θ with $\lambda = 0.4171$ Å. The patterns, recorded on an image plate (MAR 345), were processed with the software Fit2D[15] to remove Bragg reflections originating from the diamonds, the beryllium backing plates, and the tungsten gasket. After radial integration of the diffraction patterns and determination of the peak positions, the lattice parameters were refined with the program WinCSD using 11 reflections for each pressure value.[10]

EDXS and WDXS Measurements. Samples were embedded in Polyfast (Struers), metallographically polished, and then investigated with a XL 30 (Phillips) equipped with LaB_6 filament and Si(Li) detector to search for impurities. All analyses were performed at 25 kV.

For the determination of the exact composition, additional WDXS analyses were carried out with a SX 100 at 25 kV (Cameca). The pure elements were used as standards for the measurements.

DSC Measurements. Because of the sublimation of antimony, samples were encapsulated in evacuated quartz glass ampules prior to the measurements. Subsequently, the samples were measured in a STA 409 PC on a DSC/TG HIGH RG 2 measuring head (Netzsch) with a heating rate of 10 K/min. The transition temperatures were determined from the onset of the signals.

Chemical Analysis. The oxygen and nitrogen contents were determined using three samples, each of 50 to 60 mg, for every compound by the carrier gas hot-extraction method in a TC-436 DR (LECO), while the transition metal and antimony content was determined by inductively coupled plasma mass spectrometry (ICP-MS) in a PQ ExCell (TJA).

Raman Spectroscopy. Two kinds Raman spectra were recorded: spectra of powdered single crystals and polarized spectra of oriented single crystals. For the first type of measurements, finely ground powder was pressed into a thin pellet to ensure sufficient thermal conductivity. Single crystals were mounted on a goniometer head and aligned with a precision better than 0.3° by means of Weissenberg and Laue techniques (Huber, Weissenberg Goniometer 102 and Stoe, Lattice Explorer, respectively). The adjusted goniometer head was attached to the Raman spectrometer (Labram 010,

(7) Armbrüster, M. *Bindungsmodelle für intermetallische Verbindungen mit der Struktur des $CuAl_2$-Typs*; Technical University Dresden: Dresden, Germany, 2004; Cuvillier Verlag: Göttingen, Germany, 2005.
(8) Grin, Y.; Wagner, F. R.; Armbrüster, M.; Kohout, M.; Leithe-Jasper, A.; Schwarz, U.; Wedig, U.; von Schnering, H. G. *J. Solid State Chem.* **2006**, *179*, 1707−1719.
(9) Kleinke, H. *Eur. J. Inorg. Chem.* **1998**, 1369−1375.
(10) Akselrud, L. G.; Zavalii, P. Yu.; Grin, Yu.; Pecharsky, V. K.; Baumgartner, B.; Wölfel, E. *Mater. Sci. Forum* **1993**, *133*−*136*, 335−340.
(11) Sheldrick, G. M. SHELXL-97, release 97-2; University of Göttingen: Göttingen, Germany, 1997.
(12) Sheldrick, G. M. SHELXS-97, release 97−2, version WinGX; University of Göttingen: Göttingen, Germany, 1997.
(13) Farrugia, L. J. *J. Appl. Cryst.* **1999**, *32*, 837−838.
(14) Piermarini, G. J.; Block, S.; Barnett, J. D.; Forman, R. A. *J. Appl. Phys.* **1975**, *46*, 2774−2780.
(15) Hammersley, A. P.; Svensson, S. O.; Hanfland, M.; Fitch, A. N.; Häussermann, D. *High Press. Res.* **1996**, *14*, 235−248.

JobinYvon) without altering the orientation by means of a specially constructed adapter.

All Raman measurements were performed in backscattering geometry. Two notch filters for low-frequency performance allowed for the recognition of modes with small Raman shifts (>70 cm^{-1}). To avoid decomposition of the samples, the laser beam had to be attenuated by a factor of 10 before the sample. Exposures of 400 to 2000 s were conducted using an autofocus system. Twenty measurements were averaged to increase the signal-to-noise ratio. A He/Ne or an Ar laser, operating at 633 nm (15 mW) and 488 nm (50 mW), respectively, was used as an excitation source. The spectral width of the spectra is about 4 cm^{-1}, and the polarized spectra are labeled according to Porto.[16]

Hall Tensor Components and Electrical Conductivity. The two independent components of the Hall tensor were measured for each compound using single-crystalline slabs. Electrical contacts (wire, Cu 50 μm or Pt 30 μm) were fixed with silver-containing epoxy resin (Epotek H20E, Epoxy Technology) hardened at 150 °C. Subsequently, the samples were transferred to a magnet cryostat (MPMS XL7, Quantum Design), connected to a DC current source (Keithley 224, Keithley Instruments) and a nanovoltmeter (34420A, Hewlett-Packard). An isothermal series was recorded after thermal equilibration, while the magnetic field was swept from 5 to −5 T and back to zero. The labeling of the different tensor components follows the recommendation of Haussühl.[17]

Quantum Chemical Calculations. Electronic structure calculations, including band structure, density of states (DOS), and electron localization function (ELF), were performed with the TB-LMTO-ASA program package.[18] For the calculations, the experimentally determined crystal structure parameters[3] were used. Because of the small overlap of the atomic spheres, no empty spheres had to be added. The basis set consisted of the T(4s, 4p, 3d) and the Sb(5s, 5p). The Sb(5d, 4f) states were downfolded.[19] The ELF was calculated on an adequately fine mesh of 0.03 Å. Determination of the critical points, evaluation of basins, and the integration of the electron density inside these were performed numerically with the program Basin.[20] The ELF is graphically represented with the software AVS/Express.[21]

To verify the experimentally determined symmetry of the Raman modes, frozen phonon calculations based on GGA[22] were performed with the program WIEN2k.[23] The models were first geometrically optimized. The *c*/*a* ratios of the unit cells were varied by ±10% with constant cell volume, while in all the calculations, the only variable internal parameter, the *x* parameter of the position 8h, was optimized. In the next step the volume of the unit cell was varied by up to ±6%. The optimal cell parameters were determined from the plot of the calculated energies versus the volume change or the *c*/*a* ratio, respectively. Two thousand points in the asymmetric unit of the Brillouin zone were used for the calculations. The frequencies of the Raman active modes were calculated by reduction of the symmetry of the structure according to the factor group analysis (for details, see refs 7 and 8) and moving the atoms in several calculations stepwise in a range of ±0.053 Å. By plotting the acting forces, *F*, calculated after Yu et al.,[24] against the movements *x*, the force constant *D* (in N cm^{-1}) of the normal modes were determined within the harmonic approximation.[25] With the relation

$$\tilde{\nu} = 1303\sqrt{\frac{D}{m}}$$

the resulting mode frequency (cm^{-1}) was calculated (*m* = mass of the moving atom in atomic mass units).

Table 1. Composition of the Diantimonides Determined by WDXS Measurements and the Corresponding Lattice Parameters of the Sb-rich and Sb-poor Borders for TSb_2

sample composition	composition of TSb_2 by WDXS	*a* (Å)	*c* (Å)
$Ti_{20}Sb_{80}$	$Ti_{33.1(1)}Sb_{66.9(1)}$	6.6544(3)	5.8082(5)
$Ti_{40}Sb_{60}$	$Ti_{33.3(2)}Sb_{66.7(2)}$	6.6539(3)	5.8084(4)
$V_{20}Sb_{80}$	$V_{32.13(5)}Sb_{67.87(5)}$	6.5516(1)	5.6375(2)
$V_{40}Sb_{60}$	$V_{32.4(2)}Sb_{67.6(2)}$	6.5561(3)	5.6366(4)

Results and Discussion

Formation, Homogeneity Ranges, and Crystal Structure. Both compounds show dark metallic luster and are very brittle. No reaction with air has been observed, even after exposure to normal atmosphere for more than 3 years. Since the physical properties on which the chemical bonding models are based may strongly depend on the composition, it is important to determine the composition as exactly as possible. This is especially important when intermetallic compounds are involved because these often show broad homogeneity ranges and/or significant deviations from their "ideal" composition.

Therefore, the homogeneity ranges of $TiSb_2$ and VSb_2 were investigated on two-phase samples A ($T_{20}Sb_{80}$) and B ($T_{40}Sb_{60}$). The unit cell parameters and the composition of the target compounds were established in both samples and are displayed in Table 1.

The lattice parameters of titanium diantimonide in the two-phase regions on the antimony-rich and antimony-poor side are equal within one esd. This suggests a constant composition of the compound. The WDXS results confirm this and, in addition, reveal the ideal composition $TiSb_2$. According to the refined lattice parameters, vanadium diantimonide, in contrast to $TiSb_2$, exhibits a small but significant homogeneity range. The WDXS investigation of the elemental composition of the VSb_2 phase showed the vanadium-deficient composition $V_{1-x}Sb_2$ with $0.04 < x < 0.05$. Also the chemical analysis of the single crystals obtained on the Sb-rich side is in accordance with these findings ($TiSb_{2.0(1)}$ and $V_{0.90(3)}Sb_2$). The deficiency on the V site was also detected during the investigation of the crystal structure.[3]

(16) Damen, T. C.; Porto, S. P. S.; Tell, B. *Phys. Rev.* **1966**, *142*, 570−574.
(17) Haussühl, S. *Kristallphysik*; VEB Deutscher Verlag für Grundstoffindustrie: Leipzig, Germany, 1983.
(18) Jepsen, O.; Burkhardt, A.; Andersen, O. K. *The Program TB-LMTO-ASA*, version 4.7; Max-Planck-Institut für Festkörperforschung: Stuttgart, Germany, **2000**.
(19) Lambrecht, W. R. L.; Andersen, O. K. *Phys. Rev. B: Condens. Matter Mater. Phys.* **1986**, *34*, 2439−2449.
(20) Kohout, M. *Basin*, version 2.3; Max-Planck-Institut für Chemische Physik fester Stoffe: Dresden, Germany, 2001.
(21) *AVS/Express Visualization Edition*, version 5.0 R992fcs; AVS: Waltham, MA, 1998.
(22) Perdew, J. P.; Burke, K.; Ernzerhof, M. *Phys. Rev. Lett.* **1996**, *77*, 3865−3868.
(23) Blaha, P.; Schwarz, K.; Madsen, G. K. H.; Kvasnicka, D.; Luitz, J. *WIEN2k*; Institute for Materials Chemistry, TU Vienna: Vienna, Austria, 2001.
(24) Yu, R.; Singh, D.; Krakauer, H. *Phys. Rev. B: Condens. Matter Mater. Phys.* **1991**, *43*, 6411−6422.
(25) Weidlein, J.; Müller, U.; Dehnicke, K. *Schwingungsspektroskopie*; Thieme: Stuttgart, Germany, 1988.

Table 2. Data Collection and Handling for $TiSb_2$ and $V_{0.96}Sb_2$ after Annealing at 150 °C

	$TiSb_2$	$V_{0.96}Sb_2$
cryst size (mm^3)	0.2 × 0.2 × 0.2	0.2 × 0.2 × 0.2
lattice parameters (Å)	$a = 6.660(5)$	$a = 6.562(5)$
	$c = 5.818(5)$	$c = 5.643(5)$
V ($Å^3$)	258.1(4)	243.0(3)
ρ_{calcd} (g cm^{-3})	7.50	8.05
space group	*I*4/*mcm*	*I*4/*mcm*
μ (mm^{-1})	23.41	25.42
F(000)	496	500
2θ range (deg)	4.33−71.75	4.39−71.06
h, *k*, *l*	−17 to 13,	−17 to 15,
	−16 to 17,	−13 to 11,
	−12 to 8	−14 to 11
reflns	3526	3242
independent reflns	606	646
params	8	10
GOF	1.208	1.037
R1, wR2 ($I > 2\sigma I$)	0.026, 0.060	0.032, 0.074
R1, wR2 (all data)	0.027, 0.060	0.033, 0.075
extinction coeff	0.155(5)	0.059(2)
$\Delta\rho_{min}$, $\Delta\rho_{max}$ (e $Å^{-3}$)	−3.51, 3.19	−4.09, 6.64

Table 3. Atomic and Displacement Parameters for $TiSb_2$ (Upper Lines) and $V_{0.96}Sb_2$ (Lower Lines) after Annealing at 150 °C

atom	site	*x*	*y*	*z*	U_{eq}	SOF
T	4*a*	0	0	1/4	0.00424(8)	1.0
		0	0	1/4	0.0071(1)	0.96(5)
Sb	8*h*	0.15156(1)	$x + 1/2$	0	0.00555(5)	1.0
		0.15576(2)	$x + 1/2$	0	0.00752(5)	1.00(5)

atom	U_{11}	U_{22}	U_{33}	U_{12}	U_{13}	U_{23}
T	0.00397(8)	U_{11}	0.0048(2)	0	0	0
	0.0061(1)	U_{11}	0.0089(2)	0	0	0
Sb	0.00436(5)	U_{11}	0.0079(1)	0.00027(2)	0	0
	0.00648(6)	U_{11}	0.00960(7)	−0.00004(3)	0	0

Additional information about the phase boundaries was obtained by DSC measurements. The observed formation temperatures of 1000 and 901 °C for $TiSb_2$ and VSb_2, respectively, are in excellent agreement with earlier investigations.[26,27] The peritectic character of the observed signals was verified by subsequent powder X-ray diffraction experiments of the DSC samples. In addition, the liquidus temperatures could be determined to be 1080 °C for the composition $TiSb_2$ and 939 °C for VSb_2.

Havinga et al.[6] synthesized a large number of compounds crystallizing in the $CuAl_2$-type crystal structure. In their investigation, they claimed the existence of a low-temperature modification of vanadium diantimonide but did not report the crystal structure. To clarify this subject, single crystals of $V_{0.96}Sb_2$ and $TiSb_2$ were annealed in evacuated quartz glass ampoules at 150 °C for 1 year. After this period, the crystal structures were determined by means of single-crystal X-ray structure determination (Tables 2 and 3) and did not reveal significant differences to the structures determined before.[3] In addition, no signals below the peritectic formation temperatures were detected in the DSC measurements, as well as in the temperature-dependent electrical conductivity measurements.

(26) Dudkin, L. D.; Vaidanich, V. I. *Sov. Phys. Sol. State* **1960**, *2*, 377−378.
(27) Murray, J. L. Ed. Massalski, T. B. *Binary Alloy Phase Diagrams*; ASM International: Materials Park, OH, 1990.

Table 4. Relevant Interatomic Distances and PBOs in $TiSb_2$ and $V_{0.96}Sb_2$ (notation According Figure 1)

	$TiSb_2$		$V_{0.96}Sb_2$	
	length (Å)	PBO	length (Å)	PBO
*d*1(Sb−Sb)	2.852	0.88	2.885	0.78
*d*2(Sb−Sb)	3.444	0.09	3.317	0.15
*d*3(Sb−Sb)	3.535	0.06	3.479	0.08
*d*4(Sb−Sb)	3.575	0.06	3.502	0.07
*d*5(T−Sb)	2.915	0.49	2.849	0.43
*d*6(T−T)	2.904	0.36	2.818	0.23

Chemical Bonding. The shortest interatomic distances in the crystal structures of $TiSb_2$ and $V_{0.96}Sb_2$, supplemented by relevant ones according to earlier descriptions of compounds with the $CuAl_2$-type structure,[28−32] are displayed in Table 4, together with the corresponding Pauling bond orders (PBOs).[33] For the calculation of the PBO *n*, the single bond radii after Pauling[33] were used: $r(1)_{Ti} = 1.324$ Å, $r(1)_V = 1.224$ Å, and $r(1)_{Sb} = 1.41$ Å

$$D(n) = D(1) - 0.60 \log n$$

According to the PBO analysis only three distances, that are, *d*1, *d*5, and *d*6, suggest significant bonding interactions (compare also Figure 1). The *d*1 bonds form Sb_2 dumbbells, while *d*6 (T−T) forms chains oriented parallel to the crystallographic *c*-axis. In addition, interactions between the T and Sb atoms (distance *d*5) are expected. From the bond orders, the Sb_2 dumbbells are formed by a single bond, while the other interactions are significantly weaker. The distance *d*1 between the Sb atoms in the dumbbell is in the range of the reported single bond values of 2.853 Å in Zintl phases[34,35] and 2.76−2.91 Å in other intermetallic compounds.[36−38] In total, the PBO analyses for both diantimonides revealed one homoatomic T−T, one homoatomic Sb−Sb, and one heteroatomic T−Sb interaction relevant for the bonding picture. These results differ from the bonding pattern in $CuAl_2$, which shows *two* different homoatomic Al−Al interactions and one heteroatomic interaction. This was the starting point for further bonding analysis.

Since both compounds may formally be described as $T^{4+}[Sb_2]^{4-}$ within the Zintl concept,[39−43] we first performed

(28) Häussermann, U.; Lidin, S. *J. Solid State Chem.* **1997**, *132*, 151−155.
(29) Häussermann, U.; Lidin, S. *J. Solid State Chem.* **1997**, *134*, 431−431.
(30) Nowotny, H.; Schubert, K. *Z. Metallkde.* **1946**, *37*, 17−23.
(31) Pearson, W. B. *The Crystal Chemistry and Physics of Metals and Alloys*; Wiley-Interscience: New York, 1972.
(32) Schubert, K. *Kristallstrukturen zweikomponentiger Phasen*; Springer-Verlag: Berlin, Germany, 1964.
(33) Pauling, L. *The Nature of the Chemical Bond and the Structure of Molecules and Crystals*; Cornell University Press: Ithaca, New York, 1960.
(34) Emmerling, F.; Hirschle, C.; Röhr, C. *Z. Anorg. Allg. Chem.* **2002**, *628*, 559−563.
(35) von Schnering, H. G.; Hönle, W.; Krogull, G. *Z. Naturforsch. B: Chem. Sci.* **1979**, *34*, 1678−1682.
(36) Kleinke, H. *Chem. Soc. Rev.* **2000**, *29*, 411−418.
(37) Kleinke, H. *Inorg. Chem.* **2001**, *40*, 95−100.
(38) Papoian, G. A.; Hoffmann, R. *Angew. Chem.* **2000**, *112*, 2500−2544.
(39) Zintl, E. *Naturwissenschaften* **1929**, *17*, 782−783.
(40) Zintl, E.; Brauer, G. *Z. Phys. Chem. B* **1933**, *20*, 245−271.
(41) Laves, F. *Naturwissenschaften* **1941**, *29*, 244−255.
(42) Klemm, W. *Proc. Chem. Soc. London* **1958**, 329−341.
(43) Klemm, W.; Busmann, E. *Z. Anorg. Allg. Chem.* **1963**, *319*, 297−311.

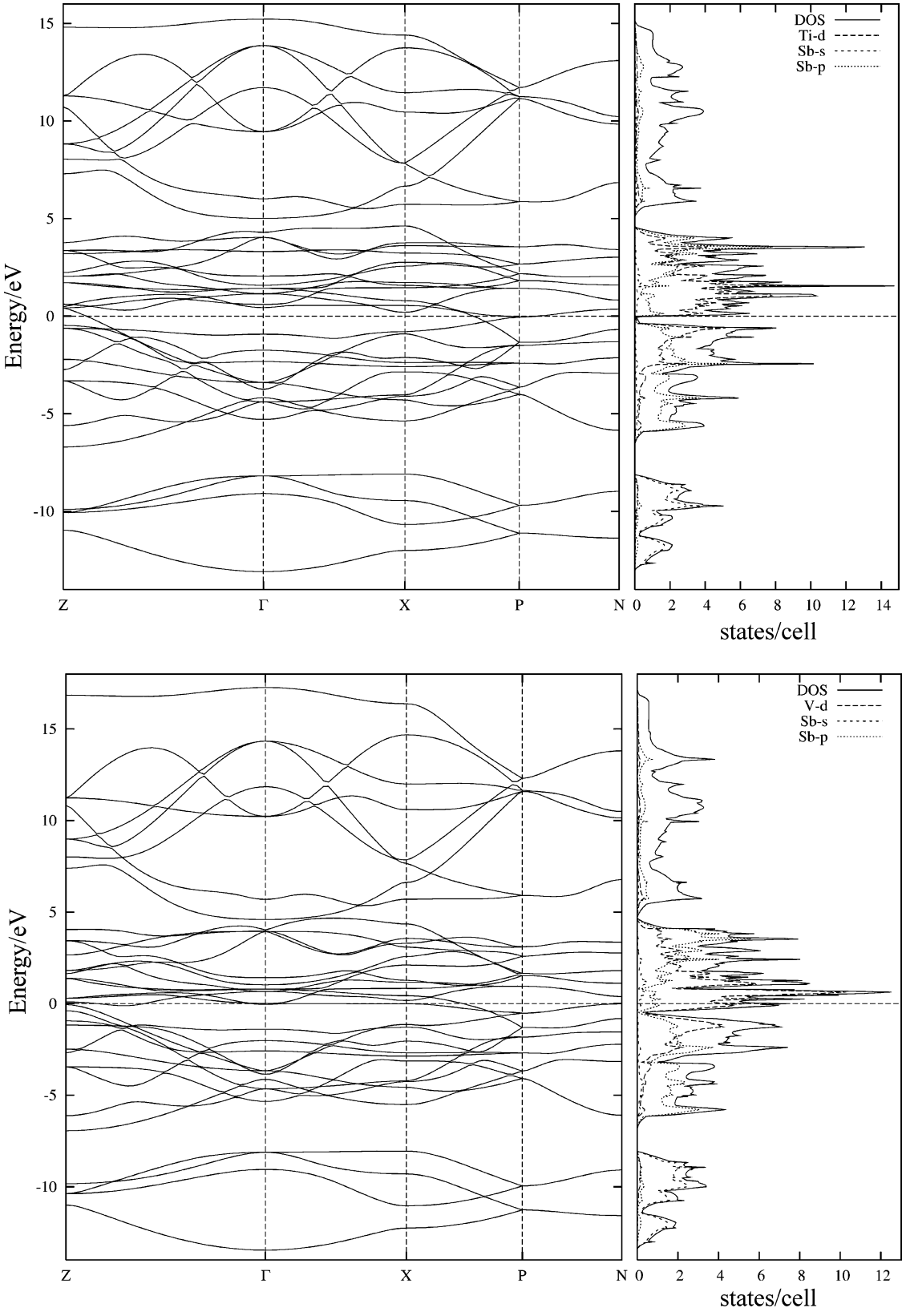

Figure 2. Electronic band structure and DOS of $TiSb_2$ (top) and VSb_2 (bottom).

calculations of the electronic band structure to prove this interpretation. The electronic density of states shows a pseudogap for $TiSb_2$, while for VSb_2, the Fermi level lies in a region of high DOS (Figure 2). However, the calculated band structure of $TiSb_2$ reveals bands crossing the Fermi energy, thus revealing metallic behavior for both compounds. According to these calculations $TiSb_2$ and $V_{0.96}Sb_2$ do not follow the Zintl concept.

To verify the findings from the band structure calculations, we measured the components of the electrical resistivity

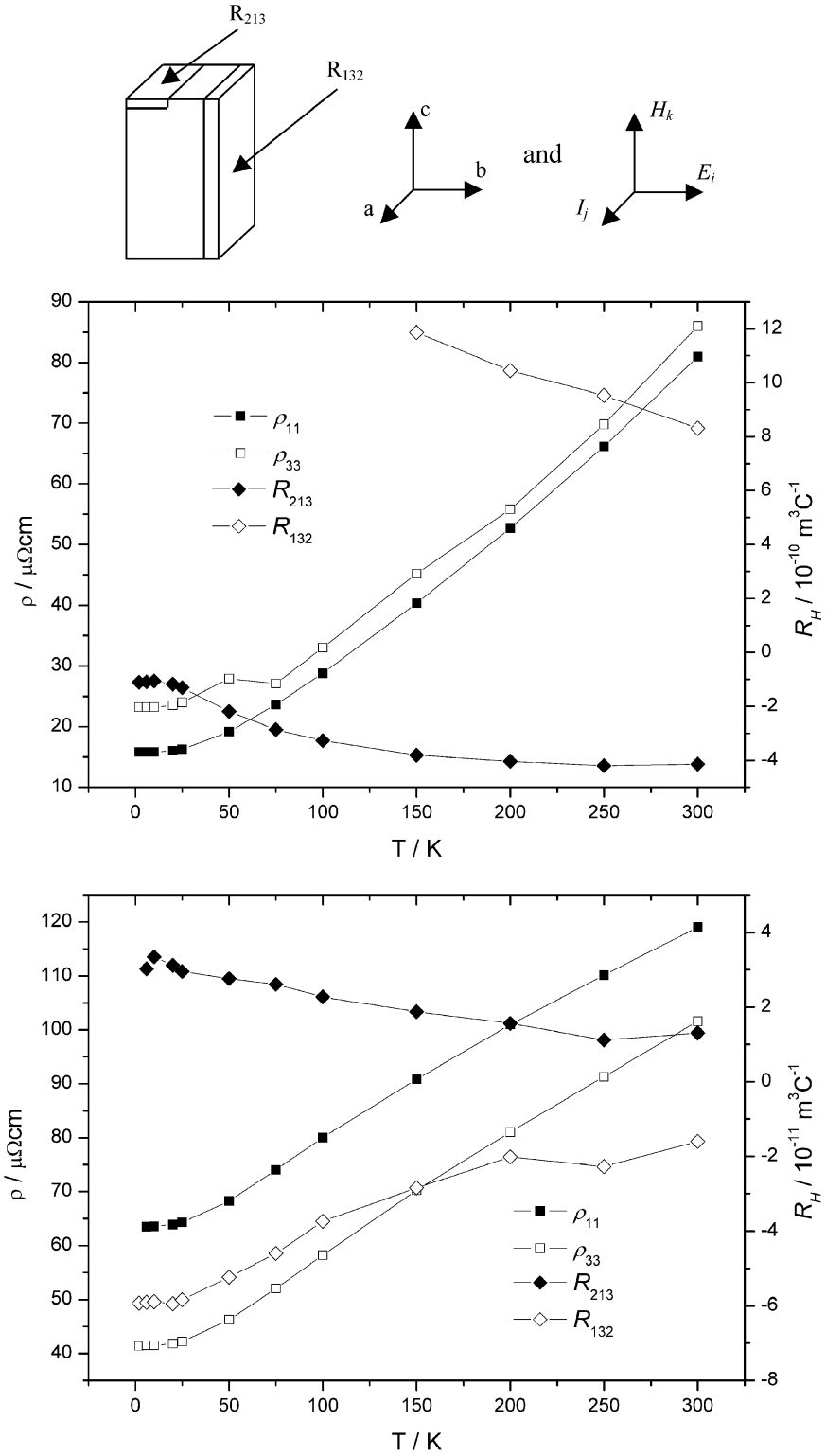

Figure 3. Orientation of the slabs for the electric conductivity measurements with the coordinate systems applied (top-middle: crystallographic system, top-right: electric system (E_i = voltage, I_j = current, and H_k = magnetic field)) and temperature dependence of the electrical resistivity and Hall tensor components of $TiSb_2$ (middle) and $V_{0.96}Sb_2$ (bottom).

tensor, ρ_{ij}, as a function of temperature. In addition, the Hall tensor components, R_{ijk}, were evaluated to compare the charge carrier concentration in the compounds. For the measurements, two single-crystalline slabs of each compound were prepared. The orientation of the slabs with respect to the crystallographic axes and the measured resistivities and Hall data are shown in Figure 3.

The data clearly show, in agreement with the band structure calculations, that neither $TiSb_2$ nor $V_{0.96}Sb_2$ can belong to the classical Zintl phases because they are not

semiconducting. Both compounds show a metal-like temperature dependence of the resistivity and room-temperature resistivities on the order of "bad" metals. By application of the single-band approximation,[44] $R_H = -(1/ne)$, to the measured Hall tensor components, the charge-carrier concentration, n, in the compounds can be estimated. As a result, $TiSb_2$ shows less than one hole for the component R_{132} and four electrons for R_{213} as charge carriers, while for $V_{0.96}Sb_2$, we calculate six electrons for R_{132} and twelve holes for R_{213}. In total, $V_{0.96}Sb_2$ exhibits more charge carriers per formula unit than $TiSb_2$ within the one-band picture. This is in good agreement with the total density of states at the Fermi level of 1.4 and 7.2 states/cell for $TiSb_2$ and VSb_2, respectively. The finding of a higher charge-carrier concentration in $V_{0.96}Sb_2$ is fully consistent with the measurements of the magnetic susceptibility by Donaldson et al.[5] The core diamagnetism is overcompensated by the magnetism of charge carriers in $V_{0.96}Sb_2$ which results in a weak temperature-independent paramagnetism of 6.1×10^{-9} emu g^{-1}, while $TiSb_2$ is diamagnetic (-1.4×10^{-9} emu g^{-1}) because of the prevalent core contribution.

A deeper insight into the chemical bonding, concerning covalent interactions, can be given by the electron localization function (ELF). The two compounds have a similar ELF topology, as can be seen from the bifurcation diagrams[45] in Figure 4. The ELF diagrams of $TiSb_2$ are shown in Figure 5.

The ELF reveals three kinds of attractors (ELF_{max} values are given in Figure 4): the highest one is located on $d1$ in a disynaptic Sb−Sb basin V^2(Sb, Sb), which has an electron count of 1.9 and 2.0 for $TiSb_2$ and VSb_2, respectively, and represents the interaction within the Sb_2 dumbbell. The second disynaptic basin (V^2(T, T), 0.2 electrons) is placed on $d6$, thus being the result of the formation of one-dimensional T chains parallel to [001]. A trisynaptic V^3(T, Sb, T) attractor, with 2.6 electrons in the basin, is located in the center of gravity of the triangle T−Sb−T, displaying a three-center interaction between the dumbbells and the T chains. In addition, the ELF states clearly, that $d2$ is not taking part in the covalent bonding, while from the PBOs alone this would remain still an issue (PBO = 0.15 for $d2$ vs 0.23 for $d6$). So a heteroatomic, three-dimensional covalently bonded network is revealed by the ELF in the diantimonides of titanium and vanadium (Figure 6).

To verify the bonding model and to determine the forces acting between the atoms, the frequencies and symmetries of the Raman-active modes can be employed for which it is necessary to perform polarized Raman measurements on oriented single crystals.

According to Laue and Weissenberg measurements, the principal axis of the single crystalline prisms is parallel to [001], while the faces parallel to it can be indexed as {100} and {110}, respectively. The factor group analysis[25,46] for

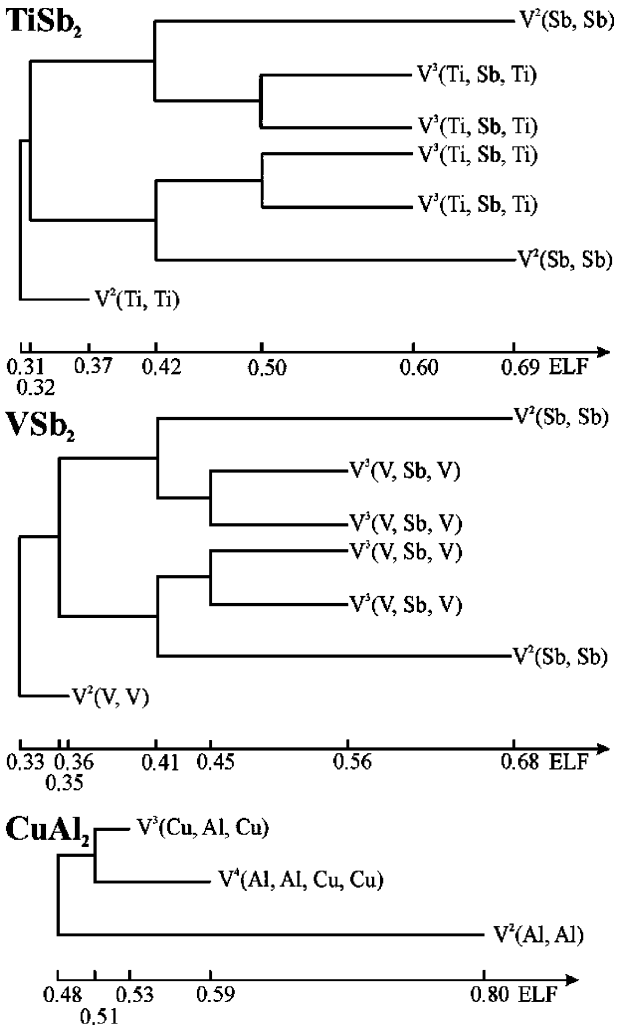

Figure 4. Bifurcation diagrams showing the identical ELF topology in $TiSb_2$ and VSb_2. For comparison the bifurcation diagram for $CuAl_2$ is added.

the isostructural compounds ($\Gamma = A_{1g} + 2A_{2g} + 2A_{2u} + B_{1g} + B_{1u} + B_{2g} + 2E_g + 3E_u$) reveals five Raman active modes ($A_{1g} + B_{1g} + B_{2g} + 2E_g$). All five modes could be measured, and the recorded Raman spectra of both compounds are shown in Figure 7. The polarized measurements on oriented single crystals allowed the determination of the symmetry of the different modes.

In addition, frozen phonon calculations have been performed to verify the mode assignment. The optimization of the crystal structures resulted in the lattice parameters $a =$ 6.6970 Å and $c = 5.8455$ Å for $TiSb_2$ and $a = 6.5799$ Å and $c = 5.6591$ Å for VSb_2. The free parameter x was calculated to 0.15279 and 0.15697 for $TiSb_2$ and VSb_2, respectively. Comparison of the optimized and measured structural parameters reveals nearly the same c/a ratio but slightly larger optimized cell volumes resulting from the use of GGA. The calculated free parameter $x = 0.15279$ ($TiSb_2$) and 0.15697 (VSb_2) agrees with the experimental value (0.15156(1) and 0.15576(2)).

In Table 5, the experimental and calculated phonon frequencies are shown. The frequencies are in very good agreement, thus verifying the symmetry assignment, except those for the B_{1g} modes. Although the corresponding

(44) Kittel, C. *Einführung in die Festkörperphysik*; Oldenbourg: München, Germany, 1999.
(45) Savin, A.; Silvi, B.; Coionna, F. *Can. J. Chem.* **1996**, *74*, 1088−1096.
(46) Rousseau, D. L.; Bauman, R. P.; Porto, S. P. S. *J. Raman Spectrosc.* **1981**, *10*, 253−290.

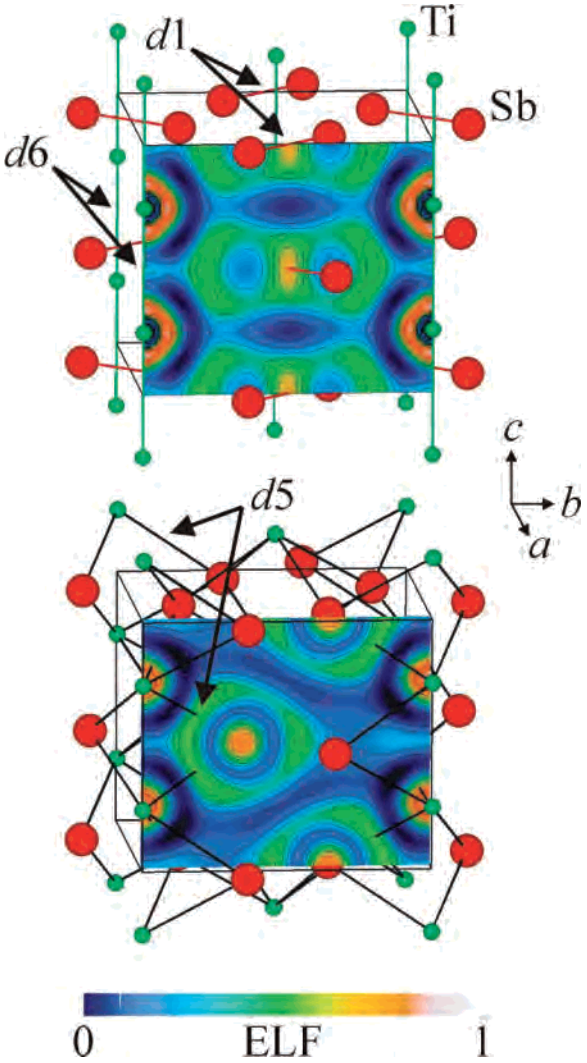

Figure 5. ELF for $TiSb_2$. The slices of the ELF are parallel to (100) and positioned at $x = 1$ and 0.875. The distance notation is according to Figure 1 and Table 4.

displacements in the quantum chemical calculations resulted in a lower energy, indicating that the structures are mechanically instable when half of the T−Sb distances are shortened, while the other half is elongated (see Figure 8 in ref 8), there is no experimental indication for a structural phase transition.

Because the positions of the covalent bonds in real space have been identified by the ELF calculations, it is possible to assign bond strengths by employing the results of the Raman measurements. After the symmetry assignment to the modes, simple harmonic force constant models have been developed with the programs Vibratz[47] and Unisoft,[48,49] and the force constants were fitted to the experimental data. As in the case of $CuAl_2$,[7,8] the three-center bond is described by a longitudinal and a transversal force constant on the *d*5 interaction. For each compound, two different models have been developed. The first model considers the interactions detected by the ELF, while

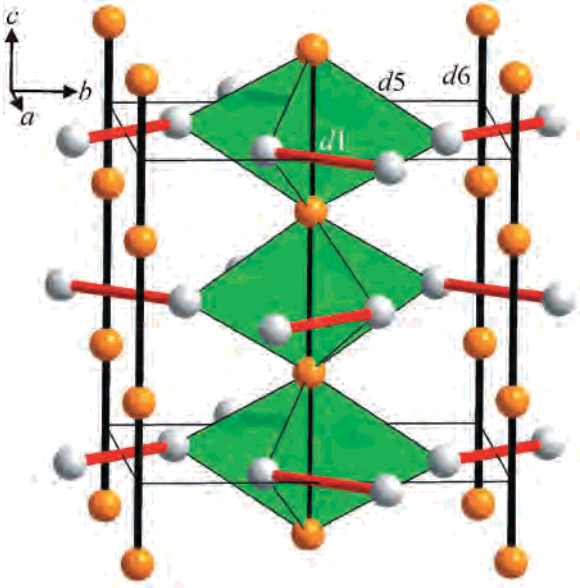

Figure 6. Model of the chemical bonding in TSb_2 (T, orange; Sb, gray). For clarity, the three-center bonds are only shown for the central chain.

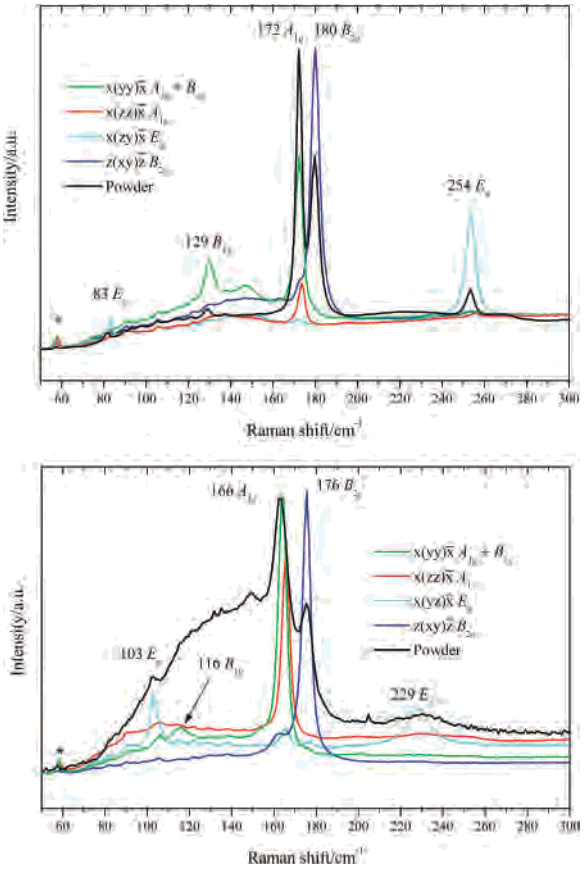

Figure 7. Raman spectra of $TiSb_2$ (top) and $V_{0.96}Sb_2$ (bottom). The polarized spectra are denoted according to the nomenclature of Porto,[16] and the allowed modes for each spectrum are given. Asterisks indicate grating ghosts.

the second employs an additional force constant on the distance *d*2, which would connect the Sb_2 dumbbells to 6^3 nets, as in the case of $CuAl_2$ (Table 6). As can be clearly seen, also according to the Raman measurements, there is no bonding interaction on *d*2. The value of this force constant

(47) Dowty, E. *VIBRATZ*, vers. 1.2; Shape Software: Kingsport, TN, 2002.
(48) Eckold, G.; Stein-Arsic, M.; Weber, H. J. *J. Appl. Crystallogr.* **1987**, *20*, 134−139.
(49) Elter, P.; Eckold, G. *Phys. B* **2000**, *276*−*278*, 268−269.

Table 5. Measured and Calculated Phonon Frequencies of the Raman Modes for $TiSb_2$ and $V_{0.96}Sb_2$

	$TiSb_2$				$V_{0.96}Sb_2$			
	measured	Wien2k	model 1[a]	model 2[a]	measured	Wien2k	model 1[a]	model 2[a]
A_{1g}	172	169	176	176	166	165	171	171
A_{2g}			99	107			110	107
A_{2g}			237	239			225	218
A_{2u}			0	0			0	0
A_{2u}			241	249			246	235
B_{1g}	129	[b]	131	129	116	[b]	113	116
B_{1u}			98	101			102	98
B_{2g}	180	174	176	176	176	176	171	171
E_g	83	106	83	83	103	115	101	103
E_g	254	249	252	254	229	232	231	229
E_u			0	0			0	0
E_u			97	102			104	100
E_u			275	277			254	251

[a] For models 1 and 2, the average esd values are 1.41 and 1.26 for $TiSb_2$ and 1.83 and 1.12 for $V_{0.96}Sb_2$. [b] See text.

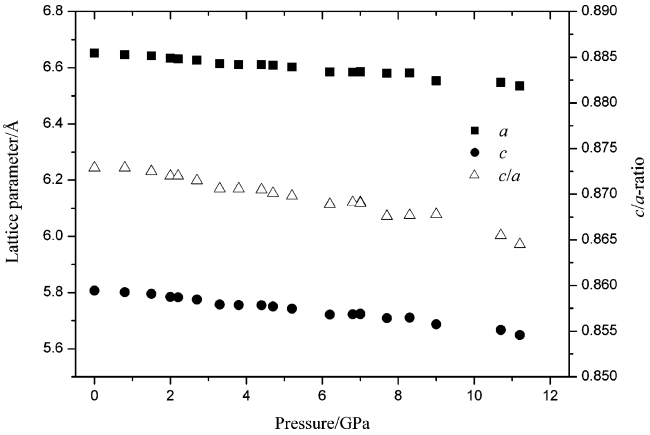

Figure 8. Pressure dependence of the lattice parameters of $TiSb_2$.

Table 6. Force Constants (N cm^{-1}) for $TiSb_2$ and $V_{0.96}Sb_2$

	$TiSb_2$			$V_{0.96}Sb_2$		
	model 1	model 2	distance (Å)	model 1	model 2	distance (Å)
*d*1 (Sb−Sb)	0.873	0.855	2.852	0.708	0.735	2.885
*d*2 (Sb−Sb)		−0.035	3.444		0.046	3.317
*d*5 (T−Sb) longitudinal	0.427	0.405	2.915	0.261	0.300	2.849
*d*5 (T−Sb) transversal	0.089	0.112		0.165	0.132	

is clearly smaller than that in $CuAl_2$, and a fit of the observed and calculated mode frequencies within the experimental error does not require this additional parameter (Table 5). For a better comparison of the two models, the standard deviations, $\tilde{\sigma}_{AM}$, are also given.

It is not possible to determine the forces acting on the distance *d*6 since a stretching along this distance does not give rise to Raman-active vibrations. All attempts to record IR spectra of the compounds (transmission and reflection) failed so that the force constant determinations are based on Raman data alone. Since the models therefore only include three or four force constants, the mechanical stability was checked by calculating the phonon dispersion. No phonon frequencies with zero or negative values were calculated, except those for the three acoustic branches at the Γ point.

The determined force constants for the Sb−Sb bond can be classified by comparison to the force constants of other compounds containing Sb−Sb single bonds. $(CH_3)_2Sb-Sb-(CH_3)_2$ and $((CH_3)_3Si)_2Sb-Sb(Si(CH_3)_3)_2$ both contain a Sb−Sb single bond with a bond length of 2.87 Å and force constants of 1.1 and 1.12 N cm^{-1}, respectively.[50] The tetrahedral Sb_4 group possesses a force constant of 1.19 Ncm^{-1}.[51,52] Despite the fact that the force constants in our compounds are slightly smaller, the Sb−Sb bond can still be described as a two-center two-electron bond. Additionally, the comparison of the vibrational frequencies of the Sb_2 dumbbells in $TiSb_2$ and VSb_2 with 166−180 cm^{-1} and the Sb_2^{4-} dumbbells in the Zintl compound Cs_4Sb_2[53] with 137 cm^{-1} (0.67 Ncm^{-1})[54] clearly reveals the difference between an isolated, highly charged Sb_2^{4-} species and the Sb_2 dumbbells in TSb_2 which are part of a three-dimensional covalent network.

There is no data for direct comparison of the three-center bond T−Sb−T available in literature. Assuming the bond strength T−X does not crucially depend on the type of transition metal, which is valid for X = H,[25] we can use the compound $(C_6H_5)_3Sb-Cr(CO)_5$[55] for comparison. The Cr−Sb vibration shows a frequency of 174 cm^{-1} from which, applying the harmonic approximation and neglecting the C-containing tails, a force constant of 0.65 N cm^{-1} can be calculated. Taking into consideration that two distances *d*5 are forming one three-center interaction, the force constant of this interaction sums up to 1.032 and 0.852 N cm^{-1} for $TiSb_2$ and $V_{0.96}Sb_2$, respectively. Thus, the heteroatomic interactions are significantly stronger than single bonds, showing bond orders of 1.6 for $TiSb_2$ and 1.3 for $V_{0.96}Sb_2$.

A comparison of the force constants, as well as the PBOs, of the two compounds reveals, that these are smaller for VSb_2 than for $TiSb_2$. This is reasonable as can be shown by comparison of the calculated DOS of the two compounds (Figure 2). If the pseudogap in $TiSb_2$ separates the bonding and antibonding states, then the additional electrons in VSb_2 have to be placed in antibonding states, which induces a weakening of the bonds.

It is not possible to get information concerning the strength of the T−T interaction from the Raman measurements, as has been pointed out before. Hence, we conducted high-pressure X-ray diffraction experiments on $TiSb_2$ to measure the compressibility of the compound. The measurements reveal a faster decrease of the *c* parameter in comparison to *a*, thus a decreasing *c*/*a* ratio with increasing pressure (Figure 8). This allows us to get qualitative information on the bond strength of the T−T bond in comparison to the three-center and two-center bonds. Because the T−T bonds are parallel to [001], they should only stiffen the compound in the

(50) Becker, G.; Freudenblum, H.; Witthauer, C. *Z. Anorg. Allg. Chem.* **1982**, *492*, 37−51.
(51) Bürger, H.; Eujen, R.; Becker, G.; Mundt, O.; Westerhausen, M.; Witthauer, C. *J. Mol. Struct.* **1983**, *98*, 265−276.
(52) Sontag, H.; Weber, R. *Chem. Phys.* **1982**, *70*, 23−28.
(53) Hirschle, C.; Röhr, C. *Z. Anorg. Allg. Chem.* **2000**, *626*, 1992−1998.
(54) Armbrüster, M.; Baitinger, M.; Baranov, A.; Grin, Y. Unpublished work.
(55) Young, F. R., III; Levenson, R. A.; Memering, M. N.; Dobson, G. R. *Inorg. Chem. Acta.* **1974**, *8*, 61−65.

[001] direction, while the Sb−Sb bonds do so in the (001) plane. With the assumption that the T−Sb−T bond has a similar compressibility in the [100] and [001] direction, the *c*/*a* ratio is a measure for the strength of the T−T bonds in comparison to that of the Sb−Sb bonds. The decreasing *c*/*a* ratio with pressure thus shows weaker T−T interactions.

Additional confirmation of the developed bonding model can be derived from the ^{121}Sb Mössbauer measurements.[5,56] Both compounds show a chemical shift of − 10.2(1) mms^{-1} relative to $Ba^{121}SnO_3$. This shift corresponds to an antimony atom showing three, mainly covalent, bonds[57,58] and thus may correspond to the three bonds in which the Sb atoms are involved (1*Sb−Sb and 2*T−Sb−T).

Conclusions

By comparison of the lattice parameters of the compounds $TiSb_2$ and VSb_2 in Sb-rich and -poor samples, it is shown, that $TiSb_2$ forms at constant composition and VSb_2 possesses a narrow homogeneity range. While WDXS measurements on $TiSb_2$ reveal an ideal 1:2 composition, the vanadium compound possesses a V deficiency and is better described as $V_{1-x}Sb_2$ ($0.04 \leq x \leq 0.05$). $TiSb_2$ and VSb_2 both form peritectically at approximately 1000 and 901 °C, respectively.

By combining experimental data and results of quantum chemical calculations, we derived a sound model of the chemical bonding in both compounds. In contrast to the isotypic compound $CuAl_2$, where the Al atoms form graphite-like 6^3 nets, the antimony atoms form isolated Sb_2 dumbbells. In addition, a covalent interaction between the T atoms (T = Ti, V) is present, which results in the formation of chains parallel to [001]. Both building groups are connected by three-center bonds T−Sb−T. This finding demonstrates a remarkable difference in the chemical bonding topology in isostructural intermetallic compounds.

The strength of the bonds in $TiSb_2$ and $V_{0.96}Sb_2$ is estimated by fitting a force constant model to Raman spectroscopic data obtained from single-crystal measurements. It reveals a single bond for the Sb_2 dumbbell and a significantly stronger T−Sb−T interaction with a bond order of 1.5. The strength of the T−T bond could not be determined. Our findings consistently show that neither $TiSb_2$ nor VSb_2 can be included in the group of Zintl compounds.

The combination of quantum chemical calculations and experimental methods allows the determination of the relevant data for the characterization of the chemical bonding, the bond location, and the bond strength and is thus a suitable method to gain insight into the chemical bonding in, especially, intermetallic compounds.

Acknowledgment. We thank M. Hanfland at ID09 (ESRF) for assistance with high-pressure X-ray diffraction and R. Cardoso-Gil for the X-ray single-crystal diffraction measurements. We acknowledge R. Ramlau and R. Niewa for WDXS and DSC investigations, respectively, as well as G. Auffermann for performing chemical analysis. F. R. Wagner is acknowledged for his assistance with the quantum chemical calculations.

Supporting Information Available: Crystallographic data in CIF format. This material is available free of charge via the Internet at http://pubs.acs.org.

IC070284P

(56) Kjekshus, A.; Nicholson, D. G. *Acta. Chem. Scand. A* **1974**, *28*, 469−470.
(57) Olivier-Fourcade, J.; Ibanez, A.; Jumas, J.-C.; Maurin, M.; Lefebvre, I.; Lippens, P. E.; Lannoo, M.; Allan, G. *J. Solid State Chem.* **1990**, *87*, 366−377.
(58) Silver, J.; Gielen, M.; Willem, R.; Wrackmeyer, B. *Solid State Organometallic Chemistry*; John Wiley & Sons: Chichester, U.K., 1999.